International Journal of Automotive Technology, Vol. ?, No. ?, pp. ?−?(year)

Serial#Given by KSAE

MODEL PREDICTIVE CONTROL BASED MULTIFUNCTIONAL ADVANCED DRIVER-ASSISTANCE SYSTEM SPECIALIZED FOR REAR-END COLLISION AVOIDANCE

Hwangjae Lee and Seibum B. Choi*

Department of Mechanical Engineering, KAIST, Daejeon 34141, Korea

(*Received date ; Revised date ; Accepted date*)

ABSTRACT− This paper presents the Model Predictive Control (MPC) based Multifunctional Advanced Driver-Assistance System (MADAS) that is optimized for rear-end collision avoidance. First, the system's operation is judged by considering the driver's intention of avoidance and the possibility of avoiding obstacle vehicles. Once the system is activated, the lateral tire force corresponding to the driver's steering input, which is essential for collision avoidance, is realized with the highest priority. The use of each tire friction circle is then maximized by utilizing available tire forces for braking through quadratic programming. While the MADAS ensures the lateral maneuver and deceleration of the vehicle, the system still can generate additional yaw moment calculated from the MPC, the upper controller, to track the driver's desired yaw rate or prevent the vehicle from becoming unstable. The nonlinearity inevitably encountered in maximizing tire forces is reflected through the extended bicycle model and the combined brushed tire model. The proposed system is verified by the vehicle dynamics software CarSim, and the simulation results show that the MADAS performs better in rear-end collision avoidance situations than conventional Advanced Driver-Assistance Systems (ADAS).

KEY WORDS : Collision avoidance, MPC, Friction circle, ADAS, Nonlinearity, Quadratic programming

NOMENCLATURE

a_x	: longitudinal acceleration
a_y	: lateral acceleration
$a_{x,max}$	: maximum longitudinal acceleration
$a_{y,max}$	: maximum lateral acceleration
m	: vehicle mass
l_f	: center of gravity-front axle distance
l_r	: center of gravity-real axle distance
I_z	: vehicle yaw moment of inertia
C_x	: tire longitudinal stiffness parameter
C_a	: tire lateral stiffness parameter
F_z	: tire normal force

1. INTRODUCTION

As traffic increases on roads, various automobile accidents have naturally occurred. To reduce this, ADAS such as Antilock Braking System (ABS) and Electronic Stability Program (ESP), which are currently installed in production vehicles, has developed rapidly. (Lie *et al*., 2006; Mirzaei and Mirzaeinejad, 2012; Huang and Chen, 2020). The new types of safety features have emerged as well over the past few years because cognitive sensors installed in vehicles have become more diverse and affordable (Bangler *et al*., 2014; Bagloee *et al*., 2016). Functions such as lane-keeping assist, lane-change assist, and lane departure warning has already been commercialized to protect drivers from the risk of accidents (Hu *et al*., 2019). In particular, more active ADAS has been proposed for rear-end collision avoidance, which accounts for a large proportion of automobile accidents (Kim *et al*., 2018; He *et al*., 2019).

Studies of such collision avoidance systems can be broadly classified into two categories. The first is Autonomous Emergency Braking (AEB), which utilizes the relative speed and distance between a host vehicle and a preceding vehicle to apply partial or full braking when a collision is imminent. Yi *et al*. (2002) studied how to optimize the brake pressure for maximum braking performance by estimating the tire-road friction during emergency braking. Diederichs *et al*. (2015) tried to

* *Corresponding author*. e-mail: sbchoi@kaist.ac.kr

consider the driver's braking intention in alarming and initiating emergency braking. However, there are limitations to the AEB. The AEB does not work when the steering by the driver is detected. Also, obstacles that cannot be avoided with the AEB can be avoided by steering in many cases (Hestermeyer *et al*., 2019).

For these reasons, the second category that has been studied for collision avoidance is Emergency Steering (ES). Most emergency steering systems have more complex algorithms than AEB. This algorithm is basically composed of two steps. Firstly, a collision-free path is created based on the host and obstacle vehicles' information. After that, the collision-free path is tracked in consideration of the driver's steering input. Choi *et al*. (2014) proposed a system in which the collision-free path is generated based on the modified trapezoidal acceleration profile, and the path is tracked using steering torque and differential braking. Hestermeyer *et al*. (2019) proposed "Evasive steering assist," and this system utilizes a preview technique for rear-end collision avoidance to provide additional steering torque when the driver's steering input is insufficient. However, in the above studies, it is difficult to reflect the intentions of all different kinds of drivers in generating the collision-free path, and it is not clear how much the driver's intentions should be reflected. In addition, the above studies focus entirely on the lateral maneuver of the vehicle during the steer-based collision avoidance and do not take the vehicle's deceleration into account. Considering that a decelerated vehicle has a higher chance of avoiding a collision and a lower fatality when the collision happens, the vehicle's deceleration should be properly implemented along with the lateral maneuver during rear-end collision avoidance by maximizing the use of available tire force.

The vehicle's stability is also essential for successful collision avoidance because the tire force is easily saturated due to a sudden maneuver during collision avoidance. Vehicle stability problems can also be caused by low tire-road friction. Here, it should be noted that the vehicle stability may conflict with the purpose of collision avoidance (Cui *et al*., 2019). Funke *et al*. (2016) proposed an algorithm that prioritizes collision avoidance over vehicle stability as needed. As such, it is essential to balance between vehicle maneuver for collision avoidance and vehicle stability at the handling limit.

In this paper, we propose the MADAS that can help a driver effectively avoid a rear-end collision considering the above-mentioned problems. When the system is first activated, the driver's steering input has the highest priority to control the lateral maneuver of the vehicle. If it is necessary to ensure the stability of the vehicle due to either excessive steering or low tire-road friction, the vehicle control is performed considering the driver's steering intention and the stability of the vehicle in a balanced way. While the collision avoidance maneuver

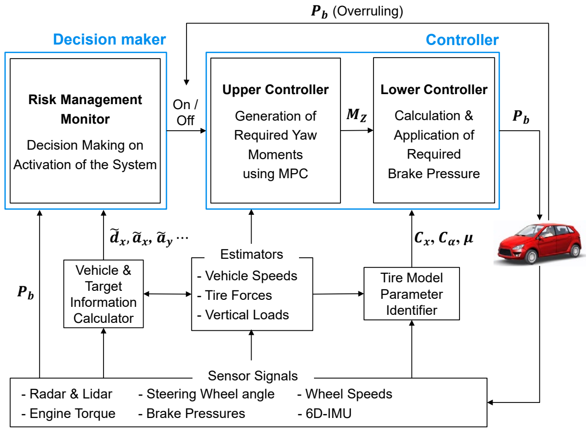

Figure 1. Flow structure of MADAS.

and the vehicle stability control are being implemented together, the available tire force is fully utilized for longitudinal deceleration by maximizing the use of the tire friction circle. The nonlinearity of tire force that must be considered to maximize the use of tire friction circle is reflected through the extended bicycle model and the combined brushed tire model. Overall, the lateral maneuver from the driver's steering input, stability control, and longitudinal deceleration are simultaneously and harmoniously performed by the single system.

This paper is constructed as follows. The overall system architecture is described in Section 2. The risk management monitor, which forms a part of the system, is covered in section 3. Tire and vehicle models to handle nonlinearities are described in Section 4, and the upper and lower controllers of the system are dealt with in Section 5. In Section 6, we analyze the proposed system through CarSim and conclude the paper in Section 7.

2. STRUCTURE OF THE SYSTEM

The MADAS is composed of the crisis management monitor, the upper controller, and the lower controller as shown in Figure 1. The risk management monitor determines whether the entire system should be activated by considering the driver's brake pressure P_b , the distance between the host vehicle and the target vehicle $\tilde{d}_x$, the longitudinal and horizontal relative accelerations $\tilde{a}_x$, $\tilde{a}_y$, and other additional information. Since the driver has the priority to operate the vehicle, the operating system can be overruled at any time with additional brake pressure when the driver determines that the operation of the system is unnecessary. In this case, the driver can get help from the conventional ADAS such as ABS and ESP.

The controller is comprised of the upper controller and the lower controller. The upper controller that is based on Model Predictive Control (MPC) generates the yaw moment M_z to track the desired yaw rate derived from the driver's steering intention when the vehicle is stable.

Serial#Given by KSAE

When it is necessary to stabilize the vehicle due to excessive steering or low tire-road friction during collision avoidance, yaw rate tracking required for collision avoidance and side slip angle tracking for vehicle stabilization are performed simultaneously and the upper controller generates the corresponding yaw moment to meet these goals.

The lower controller performs two types of brake pressure control simultaneously: the brake pressure control to realize the yaw moment generated by the upper controller and the brake pressure control to decelerate using the available tire force secured by the concept of tire friction circle. The appropriate tire model is necessary to maximize the use of each tire force. In order to utilize the tire model applied in this paper, the tire longitudinal stiffness parameter, the tire lateral stiffness parameter, and the tire-road friction coefficient μ are obtained through the tire model parameter identifier (Choi *et al*., 2013).

3. RISK MANAGEMENT MONITOR

The risk management monitor decides whether the system should be activated or not according to the algorithm shown in Figure 2. When the brake pressure is transmitted from the driver, the Braking Requirement Index (BRI) that judges the need of AEB is calculated based on the information from the vehicle sensors. Theoretically, if this value is less than 1, the collision can be avoided by braking only, and thus the AEB is activated. However, if this value is greater than 1, the collision can no longer be avoided by braking alone. Therefore, the risk management monitor additionally calculates the Steering Requirement Index (SRI), which determines the necessity of lateral maneuver. If this value is less than 1, it is possible to avoid the collision with the preceding vehicle through the lateral maneuver. Therefore, the MADAS is activated to not only implement the lateral maneuver intended by the driver to the fullest but decelerate longitudinally. On the other hand, if SRI is greater than 1, it is difficult to avoid the collision through any possible input, and the driver's input is reflected in the vehicle as it is.

BRI and SRI used in the risk management monitor algorithm are calculated as follows (Brannstrom *et al*., 2008):

$$\mathrm{BRI} = \frac{a_x + \tilde{a}_x - \dfrac{\tilde{v}_x^2}{2\tilde{x}}}{-a_{x,\max}} \tag{1}$$

$$\mathrm{SRI} = \frac{a_y + \tilde{a}_y + \dfrac{2}{t_{\mathrm{TTC}}^2}\left(\tilde{y} + \dfrac{w_h + w_t}{2} + \tilde{v}_y t_{\mathrm{TTC}}\right)}{a_{y,\max}} \tag{2}$$

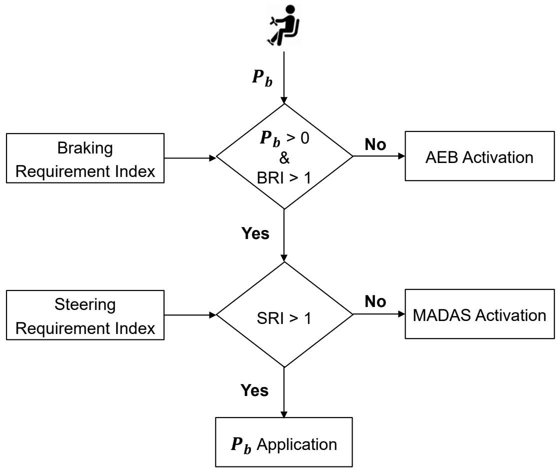

Figure 2. Risk management monitor algorithm.

where $\tilde{v}_x$ and $\tilde{x}$ are the longitudinal relative velocity and position between the host vehicle and the obstacle vehicle. $\tilde{v}_y$ and $\tilde{y}$ are the lateral relative velocity and position; w_h and w_t are the widths of the host and obstacle vehicle, respectively. Time to collision t_{TTC} in Equation (2) is also expressed as follows (Jansson, 2005):

$$t_{\mathrm{TTC}} = \begin{cases} -\dfrac{\tilde{d}_x}{\tilde{v}_x}, & \tilde{v}_x < 0 \text{ and } \tilde{a}_x = 0 \\ -\dfrac{\tilde{v}_x}{\tilde{a}_x} - \dfrac{\sqrt{\tilde{v}_x^2 - 2\tilde{a}_x\tilde{d}_x}}{\tilde{a}_x}, & \tilde{v}_x < 0 \text{ and } \tilde{a}_x \neq 0 \\ -\dfrac{\tilde{v}_x}{\tilde{a}_x} + \dfrac{\sqrt{\tilde{v}_x^2 - 2\tilde{a}_x\tilde{d}_x}}{\tilde{a}_x}, & \tilde{v}_x \geq 0 \text{ and } \tilde{a}_x < 0 \end{cases} \tag{3}$$

4. VEHICLE MODEL

4.1. Extended Bicycle Model for Tire Force Nonlinearity

The basic bicycle model is frequently used to describe the lateral dynamics of a vehicle. The left and right two wheels are lumped into the one wheel, as shown in Figure 3. Using the basic bicycle model, the lateral dynamics of a vehicle can be expressed as follows:

$$mv_x\left(\dot{\beta} + \gamma\right) = F_{yf} + F_{yr} \tag{4}$$

$$I_z\dot{\gamma} = l_f F_{yf} - l_r F_{yr} + M_z \tag{5}$$

where β and γ are the the vehicle's side slip angle and yaw rate; F_{yf} and F_{yr} stand for the front and rear lateral tire force respectively. F_{yf} and F_{yr} can also be approximated as a linear function for tire slip angle as follows:

Serial#Given by KSAE

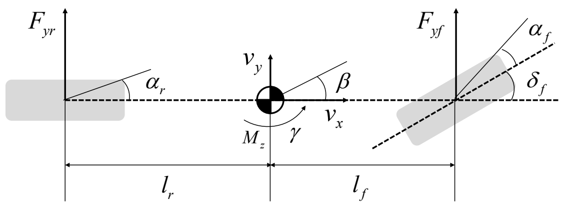

Figure 3. Basic bicycle model for vehicle lateral dynamics.

$$F_{yf} = C_f \alpha_f \tag{6}$$

$$F_{yr} = C_r \alpha_r \tag{7}$$

where C_f and C_r denote the cornering stiffness of the front and rear tires; α_f and α_r are the tire slip angles of the front and rear tires respectively.

In particular, the cornering stiffness means the slope of the lateral tire force curve in the linear region. As shown in Figure 4, Equations (6) and (7) can express the tire characteristics well when the tire exhibits linear characteristics. However, errors are bound to occur when it enters the nonlinear region. Therefore, the lateral tire force curve is locally linearized with respect to the current operating point to consider the nonlinearity of tires. Then, the equations that can be applied to both the linear and nonlinear regions are expressed as follows (Choi and Choi, 2014);

$$F_{yf} = C_{f0}\alpha_f + F_{yf0} \tag{8}$$

$$F_{yr} = C_{r0}\alpha_r + F_{yr0} \tag{9}$$

where C_{f0} and C_{r0} are the slopes of the lateral tire force curve at the current tire side slip angle α_f and α_r; F_{yf0} and F_{yr0} are the residual tire forces as shown in Figure 4.

Considering that α_f and α_r have the following relations:

$$\alpha_f = \delta_f - \left(\beta + \frac{l_f r}{v_x}\right),\ \alpha_r = -\beta + \frac{l_r \gamma}{v_x} \tag{10}$$

where δ_f and β are the steering angle and side slip angle, the extended bicycle model that reflects the nonlinearity of tire force can be obtained by combining Equations (4) ~ (10), as follows:

$$\begin{aligned} \dot{x} &= Ax + B_\delta \delta_f + B_M M_z + E_{add} \\ y &= Cx \end{aligned} \tag{11}$$

where

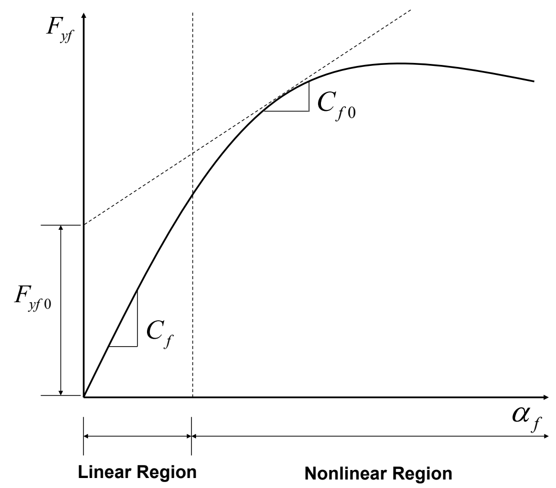

Figure 4. Lateral tire force curve.

$$x = \begin{bmatrix} \beta & \gamma \end{bmatrix}^T$$

$$A = \begin{bmatrix} -\dfrac{C_{f0}+C_{r0}}{mv_x} & \dfrac{C_{r0}l_r - C_{f0}l_f}{mv_x^{\,2}} - 1 \\ \dfrac{C_{r0}l_r - C_{f0}l_f}{I_z} & -\dfrac{C_{f0}l_f^{\,2} + C_{r0}l_r^{\,2}}{I_z v_x} \end{bmatrix},\ B_\delta = \begin{bmatrix} \dfrac{C_{f0}}{mv_x} \\ \dfrac{C_{f0}l_f}{I_z} \end{bmatrix}$$

$$B_M = \begin{bmatrix} 0 \\ \dfrac{1}{I_z} \end{bmatrix},\ E_{add} = \begin{bmatrix} \dfrac{F_{yf0}+F_{yr0}}{mv_x} \\ \dfrac{l_f F_{yf0} - l_r F_{yr0}}{I_z} \end{bmatrix},\ C = \begin{bmatrix} 1 & 0 \\ 0 & 1 \end{bmatrix}$$

4.2. Tire Model

In order for the vehicle model developed in the previous section to reflect the nonlinearity of tires, a tire model that expresses the nonlinearity well is also needed. Therefore, the following longitudinal and lateral combined brushed tire model, which can represent tire nonlinearity close to reality, is applied (Pacejka, 2006; Hsu, 2009):

$$F_{x,i} = \frac{C_x\left(\dfrac{\lambda_i}{1+\lambda_i}\right)}{f_i}F_i,\ F_{y,i} = -\frac{C_\alpha\left(\dfrac{\tan\alpha_i}{1+\lambda_i}\right)}{f_i}F_i \tag{12}$$

where

$$F_i = \begin{cases} f_i - \dfrac{1}{3\mu F_{z,i}} f_i^2 + \dfrac{1}{27\mu^2 F_{z,i}^{\,2}} f_i^3 & \text{if } f_i \le 3\mu F_{z,i} \\ \mu F_{z,i} & \text{otherwise} \end{cases}$$

$$f_i = \sqrt{C_x^{\,2}\left(\frac{\lambda_i}{1+\lambda_i}\right)^2 + C_\alpha^{\,2}\left(\frac{\tan\alpha_i}{1+\lambda_i}\right)^2}$$

In Equation (12), F_x and F_y are the tire longitudinal and lateral force respectively; λ is the tire slip ratio; subscript i stands for the ith wheel where i = 1,2,3,4 which correspond to the left-front, right-front, left-rear, and right-rear wheels respectively.

Parameters such as λ, α, and F_z can be either measured by vehicle sensors or obtained by observers. In addition to that, C_x, C_α, and μ are identified by the linearized recursive least square method (Choi *et al*., 2013). Once all parameters are determined in this way, not only the values of C_{f0}, C_{r0}, F_{yf0}, and F_{yr0} that are needed to express the vehicle model, but also the force of each wheel required by the lower controller can be obtained.

5. DESIGN OF CONTROLLERS

5.1. Upper Controller

The extended bicycle model, Equation (11), is discretized using zero-order hold as follows to formulate the MPC:

$$\begin{aligned} x_d(k+1) &= A_d x_d(k) + B_{M\_d} u(k) + E_d(k) \\ y_d(k) &= C_d x_d(k) \end{aligned} \tag{13}$$

where

$$\begin{aligned} E_d(k) &= B_{\delta\_d}\delta_{f\_d}(k) + E_{add\_d} \\ u(k) &= M_{z\_d}(k) \end{aligned}$$

Subscript d denotes a discrete matrix, and k stands for kth step in discrete time. In $E_d(k)$, $\delta_{f\_d}(k)$ is set as a time-varying variable and determined through the following equation, and the remaining terms are made constant over the prediction time span:

$$\delta_{f\_d}(k) = \delta_f(0) + k \cdot t_s \cdot \dot{\delta}_f(0) \tag{14}$$

where t_s is the sampling time.

Since the desired yaw moment we want to apply to the vehicle is the amount of change in the yaw moment according to each time step, set Δu as the manipulated variable for the output of the controller as follows (Wang, 2009):

$$\begin{aligned} x_a(k+1) &= A_a x_a(k) + B_a \Delta u(k) + E_a \Delta e(k) \\ y_a(k) &= C_a x_a(k) \end{aligned} \tag{15}$$

where

$$x_a(k+1) = \begin{bmatrix} \Delta x_d(k+1) \\ y_d(k+1) \end{bmatrix},\ A_a = \begin{bmatrix} A_d & O \\ C_d A_d & I \end{bmatrix}$$

$$B_a = \begin{bmatrix} B_d \\ C_d B_d \end{bmatrix},\ E_a = \begin{bmatrix} I \\ C_d \end{bmatrix},\ C_a = \begin{bmatrix} O & I \end{bmatrix}$$

$$\begin{aligned} \Delta x_d(k) &= x_d(k) - x_d(k-1) \\ \Delta u(k) &= u(k) - u(k-1) \\ \Delta e(k) &= E_d(k) - E_d(k-1) \end{aligned}$$

Based on the newly augmented model above, the future output variables Y can be explicitly expressed as the current state variables $x_a(k)$, the future control parameters ΔU, and the future extra terms ΔE as follows:

$$Y = F x_a(k) + G\Delta U + H\Delta E \tag{16}$$

where

$$Y = \begin{bmatrix} y_a(k+1) & y_a(k+2) & y_a(k+3) & \cdots & y_a(k+N_p) \end{bmatrix}^T$$

$$F = \begin{bmatrix} C_a A_a & C_a A_a^2 & C_a A_a^3 & \cdots & C_a A_a^{N_p} \end{bmatrix}^T$$

$$G = \begin{bmatrix} C_a B_a & 0 & 0 & \cdots & 0 \\ C_a A_a B_a & C_a B_a & 0 & \cdots & 0 \\ C_a A_a^2 B_a & C_a A_a B_a & C_a B_a & \cdots & 0 \\ \vdots & & & & \\ C_a A_a^{N_p-1} B_a & C_a A_a^{N_p-2} B_a & C_a A_a^{N_p-3} B_a & \cdots & C_a A_a^{N_p-N_c} B_a \end{bmatrix}$$

$$\Delta U = \begin{bmatrix} \Delta u(k) & \Delta u(k+1) & \Delta u(k+2) & \cdots & \Delta u(k+N_c-1) \end{bmatrix}^T$$

$$H = \begin{bmatrix} C_a E_a & 0 & 0 & \cdots & 0 \\ C_a A_a E_a & C_a E_a & 0 & \cdots & 0 \\ C_a A_a^2 E_a & C_a A_a E_a & C_a E_a & \cdots & 0 \\ \vdots & & & & \\ C_a E_a^{N_p-1} B_a & C_a E_a^{N_p-2} B_a & C_a E_a^{N_p-3} B_a & \cdots & C_a E_a \end{bmatrix}$$

$$\Delta E = \begin{bmatrix} \Delta e(k) & \Delta e(k+1) & \Delta e(k+2) & \cdots & \Delta e(k+N_p-1) \end{bmatrix}^T$$

In Equation (16), N_p and N_c are the prediction horizon and the control horizon that is set as 50 and 10 in this controller.

The final goal of the upper controller is to track the yaw rate for collision avoidance and the side slip angle for vehicle stability control, so define the cost function reflecting these control goals as follows:

$$J = (R_{ref} - Y)^T Q (R_{ref} - Y) + \Delta U^T R \Delta U \tag{17}$$

where

$$R_{ref}=\begin{bmatrix}\beta_{ref}(k+1)\\ \gamma_{ref}(k+1)\\ \vdots \\ \beta_{ref}(k+N_p)\\ \gamma_{ref}(k+N_p)\end{bmatrix},\ Y=\begin{bmatrix}\beta(k+1)\\ \gamma(k+1)\\ \vdots \\ \beta(k+N_p)\\ \gamma(k+N_p)\end{bmatrix}$$

$$Q=\begin{bmatrix} w_\beta & 0 & \cdots & & O & \\ 0 & w_\gamma & & & & \\ \vdots & & \ddots & & \vdots & \\ & & & & w_\beta & 0 \\ O & & \cdots & & 0 & w_\gamma \end{bmatrix},\ R=10^{-8}\times\begin{bmatrix}1.5 & \cdots & 0\\ \vdots & \ddots & \vdots \\ 0 & \cdots & 1.5\end{bmatrix}$$

In Equation (17), subscript ref stands for a reference; w_β and w_γ are the weighting factors for side slip angle and yaw rate respectively.

Considering the steady-state of the vehicle, β_{ref} and γ_{ref} can be derived as follows (Rajamani, 2012);

$$\beta_{ref}=\frac{l_r-\dfrac{l_f m v_x^2}{2C_r\left(l_f+l_r\right)}}{l_f+l_r+\dfrac{m v_x^2\left(l_r C_r-l_f C_f\right)}{2C_f C_r\left(l_f+l_r\right)}}\delta_f \tag{18}$$

$$\gamma_{ref}=\frac{v_x}{l_f+l_r+\dfrac{m v_x^2\left(l_r C_r-l_f C_f\right)}{2C_f C_r\left(l_f+l_r\right)}}\delta_f \tag{19}$$

C_f and C_r used in Equations (18) and (19) are the cornering stiffness in the linear region shown in Figure 4. Therefore, the required lateral behavior of the vehicle increases linearly as the driver's steering increases. Additionally, yaw rate and side slip angle that exceeds the tire-road friction limit can make the vehicle unstable, so each reference is bounded as follows considering the road adhesion (Rajamani, 2012);

$$\beta_{ref\_bound}=\tan^{-1}\left(0.02\mu g\right) \tag{20}$$

$$\gamma_{ref\_bound}=\frac{\mu g}{v_x} \tag{21}$$

where g is the gravitational acceleration.

w_β and w_γ determine how much weight would be put on either the yaw rate tracking or the side slip angle tracking considering vehicle stability. The stability of the vehicle is determined based on the side slip angle – side slip angle rate phase plane stability judgment method (Inagaki, 1995), and the respective weighting factors are set as follows:

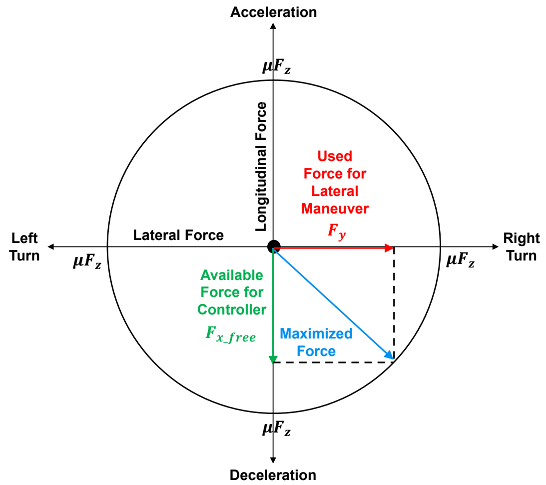

Figure 5. Tire friction circle

$$\begin{cases} w_\beta=0,\ w_\gamma=1, & \text{if } \left|\beta+B_1\dot{\beta}\right|\le B_2 \\ w_\beta=1,\ w_\gamma=1, & \text{if } \left|\beta+B_1\dot{\beta}\right|> B_2 \end{cases} \tag{22}$$

where $\dot{\beta}$ is the side slip angle rate; B_1 and B_2 are the stability boundary parameters that can be calibrated by simulation results.

Finally, the upper controller computes the cost function, Equation (17), which subjects to Equations (18) ~ (22), through quadratic programming to obtain the optimized ΔU.

5.2. Lower Controller

The lower controller utilizes the tire force to the maximum to decelerate the vehicle. In addition, it applies the yaw moment derived from the upper controller to the vehicle using the longitudinal tire force through brakes. It is necessary to determine the available tire force to achieve these goals. Using the tire friction circle shown in Figure 5, the available tire force F_{x_free} excluding the lateral tire force used in the lateral maneuver to avoid the collision is expressed as follows:

$$F_{x\_free,i}=\eta\sqrt{\left(\mu F_{z,i}\right)^2-F_{y,i}^2} \tag{23}$$

where η is the safety margin parameter. If all available tire force is used for braking without η, the coupled relationship between the longitudinal and lateral tire forces will result in less lateral maneuver than intended by the driver. This can have a significant adverse effect on rear-end collision avoidance. Therefore, η must be set so that the use of the available tire force does not interfere with the lateral maneuver. It can be expressed as a function of tire slip angle to take the lateral tire force into account. In addition, since the tire slip angle for generating a certain lateral force is affected by the tire-road friction coefficient, η considering all of them is experimentally expressed as follows:

$$\begin{cases} \eta = 0.9, & \text{if } |\alpha_i| \le 0.1\mu \\ \eta = 0.3, & \text{otherwise} \end{cases} \tag{24}$$

Once the available tire force has been determined, the longitudinal braking should be performed not only for the deceleration of the vehicle but for the realization of the yaw moment derived from the upper controller. The yaw moment derived from the upper controller is generated by the longitudinal tire force through brakes, and the related expression is as follows:

$$\begin{aligned} M_z = & \left(-\frac{d}{2}\cos(\delta_f) + l_f \sin(\delta_f)\right)F_{x,1} + \left(-\frac{d}{2}\right)F_{x,3} \\ & + \left(\frac{d}{2}\cos(\delta_f) + l_f \sin(\delta_f)\right)F_{x,2} + \left(\frac{d}{2}\right)F_{x,4} \end{aligned} \tag{25}$$

where d is the width of the vehicle. A planal vehicle model, not the bicycle model, should be used to derive Equation (25). Related information can be referred to Zhai, 2016.

Finally, the cost function of the lower controller to achieve both goals of applying the required yaw moment through the longitudinal tire force and using the available tire force to decelerate can be expressed as follows by combing Equations (23) ~ (25):

$$\begin{aligned} & J = (F_{ref} + F)^T (F_{ref} + F) \\ & \text{subject to} \\ & SF = M_z,\ -F_{ref} \le F \le 0 \end{aligned} \tag{26}$$

where

$$F_{ref} = \begin{bmatrix} F_{x\_free,1} \\ F_{x\_free,2} \\ F_{x\_free,3} \\ F_{x\_free,4} \end{bmatrix},\ F = \begin{bmatrix} F_{x,1} \\ F_{x,2} \\ F_{x,3} \\ F_{x,4} \end{bmatrix},$$

$$S = \begin{bmatrix} -\frac{d}{2}\cos(\delta_f) + l_f \sin(\delta_f) \\ \frac{d}{2}\cos(\delta_f) + l_f \sin(\delta_f) \\ -\frac{d}{2} \\ \frac{d}{2} \end{bmatrix}$$

Type	Applied ADAS
Type 1	MADAS
Type 2	ESP
Type 3	ABS
Type 4	ESP + ABS

Table 1. Applied ADAS according to each type.

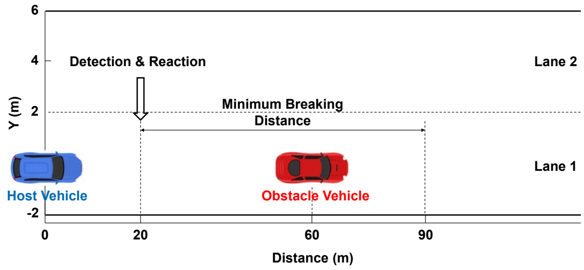

Figure 6. Collision avoidance scenario 1.

F in Equation (26) can be obtained using quadratic programming. The obtained F is the longitudinal tire force to be applied to the vehicle, which can be applied to the vehicle through the brake pressure of each wheel and it has the following relation:

$$P_{b,i} = \frac{F_{x,i}}{K_i} \tag{27}$$

where P_b and K denote the required cylinder brake pressure and brake gain respectively.

6. SIMULATION ANALYSIS

The performance of MADAS was evaluated using the front-wheel driving B-class hatchback model in the high-fidelity simulation software, CarSim, in conjunction with MATLAB/Simulink. The MADAS is compared with the conventional ADAS, as shown in Table 1, to objectively verify the rear collision avoidance performance of the MADAS. Two scenarios are set for the simulation. In the first scenario, the host vehicle requires a single lane change to avoid a collision with the obstacle vehicle in the same lane. In the second scenario, the host vehicle requires a double lane change to avoid a collision with the obstacle vehicles detected in both lanes. The ideal trajectory for collision avoidance is generated for each scenario, and the driver model built into CarSim is used as the driver. In both scenarios, it is assumed that the obstacle vehicles are suddenly detected 40 m ahead, and the driver attempts the evasive maneuver by steering and braking simultaneously excepts Type 2 (Steering only). Additionally, in order to describe a situation in which rear collision avoidance occurs frequently, the tire-road

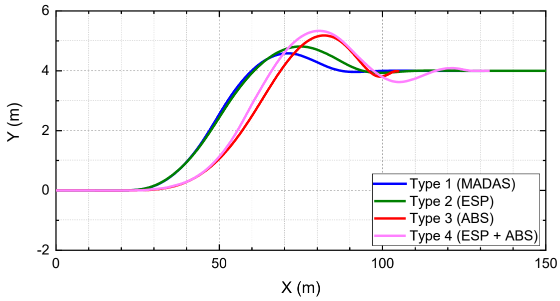

(a) Trajectory

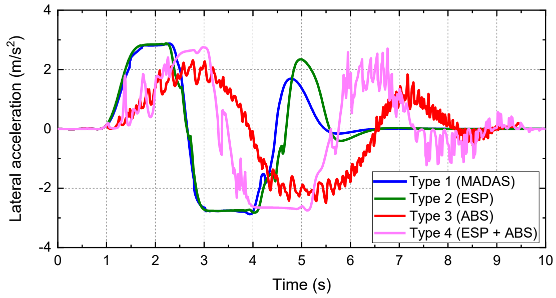

(b) Lateral acceleration

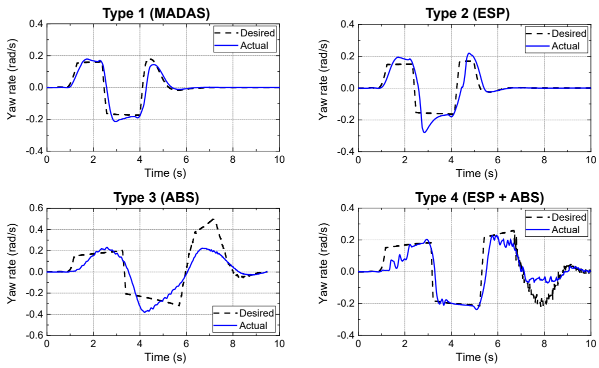

(c) Yaw rate

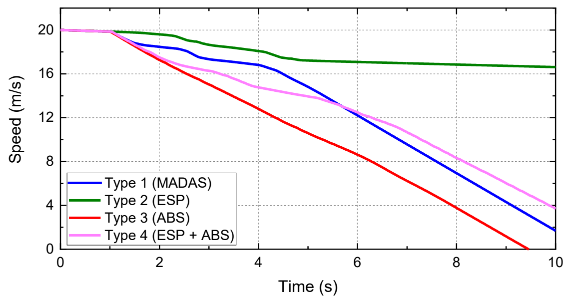

(d) Longitudinal speed

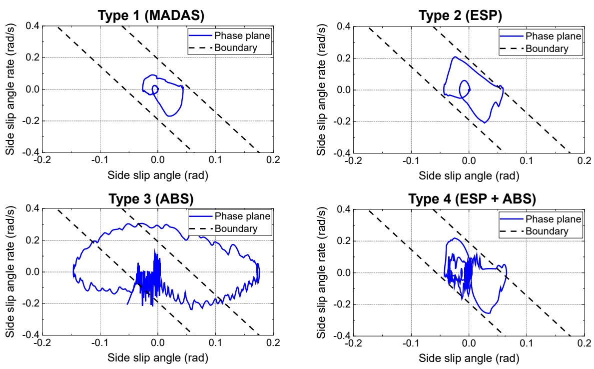

(e) $\beta - \dot{\beta}$ phase plane

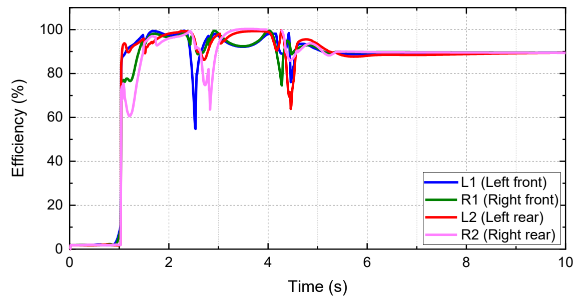

(f) Tire force efficiency of Type 1

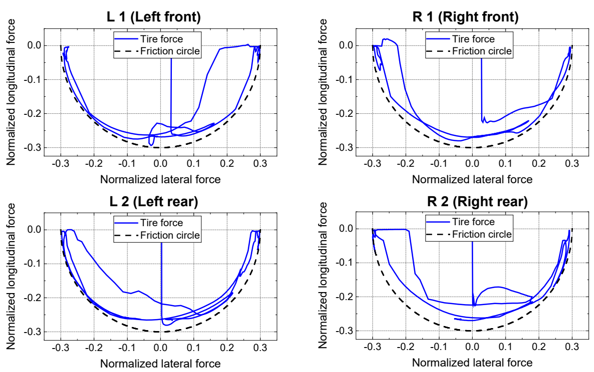

(g) Tire force friction circle of Type 1

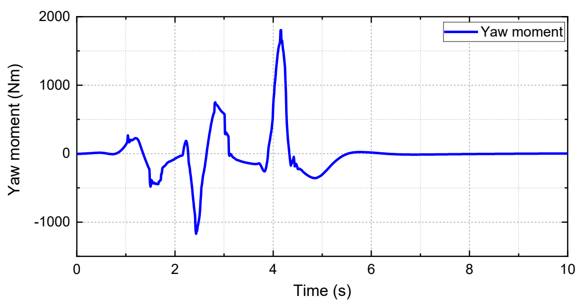

(h) Generated yaw moment of Type 1

Figure 7. Simulation results for collision avoidance scenario 1.

friction coefficient is set to 0.3, and the speed of the host and the obstacle vehicles are set to 20 m/s and 0 m/s respectively. Finally, even if the host vehicle impacts the obstacle vehicle or the road boundary, the simulation continues for analysis.

6.1. Avoiding One Obstacle (Single Lange Change)
The first scenario is shown in Figure 6. The MADAS is triggered at 20 m by the risk management monitor. The ESP and ABS are also activated based on the conventional activation criteria for each system. The overall simulation results for rear-end collision avoidance are shown in Figure 7. According to the trajectory shown in Figure 7(a), Type 1 and Type 2 succeed in avoiding rear-end collisions. On the other hand, Type 3 impacts the rear of the obstacle vehicle and the left road boundary, while Type 4 impacts the left road boundary.

In the case of Type 3 and Type 4, which have the aid of ABS, the driver's intended lateral maneuver is not fully executed at the beginning due to the longitudinal and lateral tire force coupling effect, as shown in Figures 7(b) ~ (d). On the other hand, Type 1 tracks the driver's desired yaw rate better and generates almost maximum lateral acceleration as much as Type 2 to avoid the collision. In addition, Type 1, unlike Type 2, decelerates the vehicle as well, and the deceleration is comparable with Type 3. As shown in Figure 7(e), Type 1 can also successfully perform the vehicle stability control, and its performance is superior to other Types equipped with the ESP.

The MADAS maximizes the use of tire force with extremely high efficiency during the entire collision avoidance maneuver, as shown in Figure 7(f). This can also be confirmed through the fact that the normalized force of each wheel is mapped very close to the limit of the friction circle, as shown in Figure 7(g). It is sometimes seen that the normalized force of each wheel does not reach the limit of the friction circle, which might be mistaken as a defect of the system. However, it is definitely the intended outcome from the controllers because it proves that the MADAS is successfully applying the required yaw moment to the vehicle. For example, as shown in Figures 7(f) ~ (h), the efficiency of L1, left front wheel, temporarily decreases at around 2.5 seconds. This is because the application of the brake pressure of L1 is temporarily suspended. Accordingly, the negative required yaw moment is applied to the vehicle due to the difference in the longitudinal force of both side wheels.

6.2. Avoiding Two Obstacles (Double Lange Change)
The second scenario is shown in Figure 8, and the operation of the MADAS starts at 20 m by the risk management monitor and continues until the both

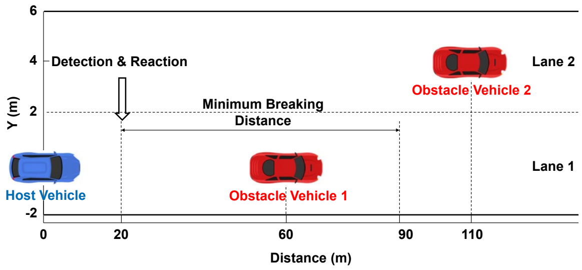

Figure 8. Collision avoidance scenario 2.

obstacle vehicles are avoided. The overall simulation results for rear-end collision avoidance are shown in Figure 9. Only Type 1 successfully avoids two obstacle vehicles without any collision while Type 2 collides with the right road boundary; Type 3 collides with the first obstacle vehicle and the left road boundary; Type 4 collides with the left and right road boundaries as shown in Figure 9(a).

In Figures 9(b) ~ (d), Type 1 helps achieve steady deceleration while realizing the driver's steering intention to the maximum. Type 2 implements the driver's lateral maneuver intention well but shows poor braking performance. Type 3 and Type 4 cannot fully realize the driver's lateral maneuver intention in the first place because the goal of ABS conflicts with the goal of collision avoidance sometimes. Figure 9(e) shows that Type 1 also offers the best performance in maintaining vehicle stability. In the case of Type 2 ~ 4, the phase plane plot occasionally crosses the boundary.

Figure 9(f) shows that the MADAS harmoniously uses the lateral and longitudinal tire force throughout the collision avoidance and attains a high level of tire force efficiency all the time. Comparing Figure 9(g) with Figures (f) and (h), one can notice that the MADAS uses the tire friction circle to the maximum and applies the required yaw moment to the vehicle by adjusting the brake pressure of each wheel as needed.

7. CONCLUSION

In this paper, the multifunctional advanced driver-assistance system specialized for rear-end collision avoidance was developed and evaluated in the CarSim simulation environment. The proposed system highlights the following unique points from the previously reported methods;

(1) Lateral maneuver intended by the driver's steering input is realized without any interruption, and available tire forces are used to the maximum to decelerate the vehicle.
(2) It utilizes the structural advantages of MPC to achieve a balance between collision avoidance and vehicle stability control according to the situations.

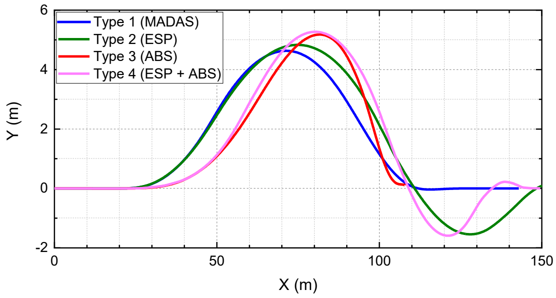

(a) Trajectory

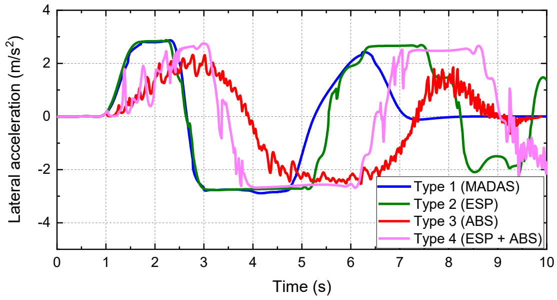

(b) Lateral acceleration

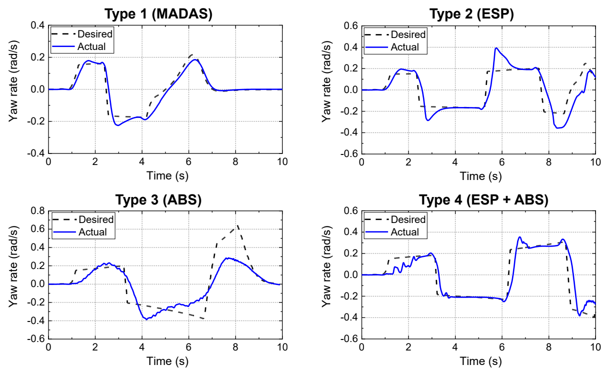

(c) Yaw rate

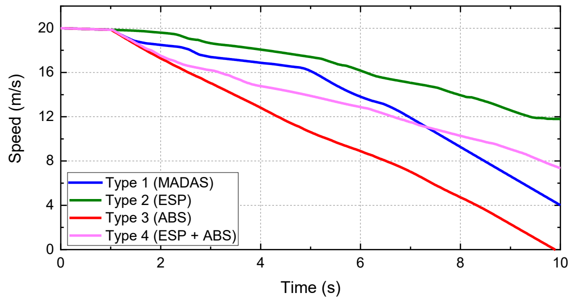

(d) Longitudinal speed

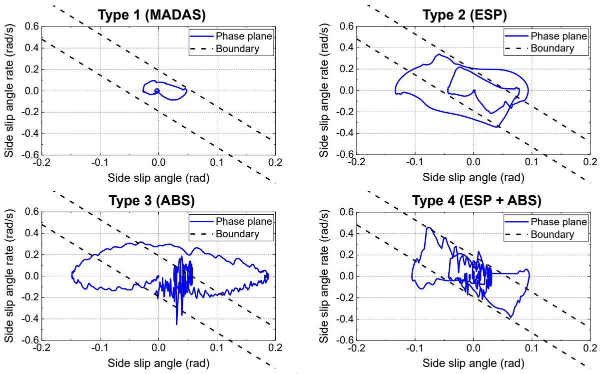

(e) $\beta - \dot{\beta}$ phase plane

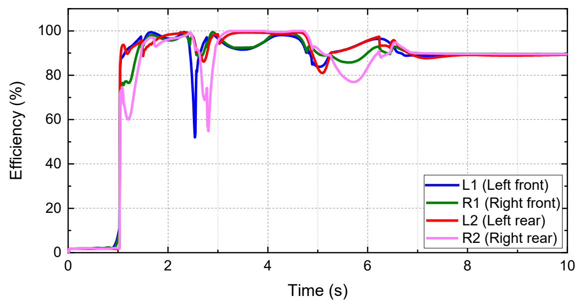

(f) Tire force efficiency of Type 1

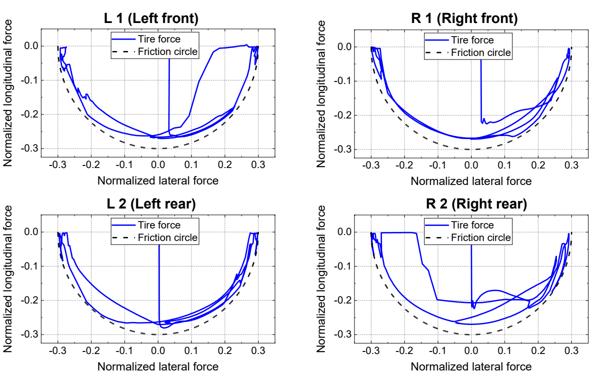

(g) Tire force friction circle of Type 1

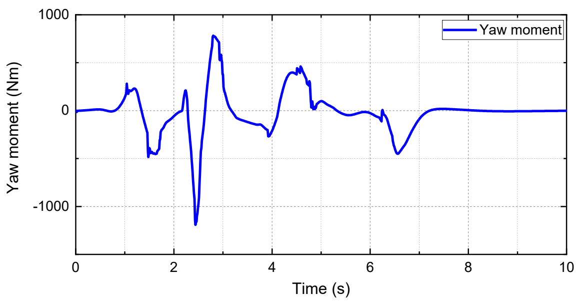

(h) Generated yaw moment of Type 1

Figure 9. Simulation results for collision avoidance scenario 2.

(3) It uses the model and controllers taking the tire nonlinearity into account to maximize the use of the tire force.
(4) The vehicle's lateral maneuver, braking, and stability control are integrated into the one system in a balanced way to achieve the goal of rear-end collision avoidance without infringing on each other's unique functions.

The simulation results prove that the proposed system performs better in rear-end collision avoidance situations than conventional ADAS-equipped vehicles.

ACKNOWLEDGEMENT−This research was partly supported by the BK21+ program through the NRF funded by the Ministry of Education of Korea; the Technology Innovation Program (20010263, Development of innovative design for UX environment improvement and commercialization model of wheelchair electric motorization kit with enhanced portability and convenience) funded By the Ministry of Trade, Industry Energy (MOTIE, Korea); the National Research Foundation of Korea (NRF) grant funded by the Korea government (MSIP) (No. 2020R1A2B5B01001531); the Technology Innovation Program (20014983, Development of autonomous chassis platform for a modular vehicle) funded By the Ministry of Trade, Industry Energy (MOTIE, Korea).

REFERENCES

Bagloee, S.A., Tavana, M., Asadi, M. and Oliver, T. (2016). Autonomous vehicles: challenges, opportunities, and future implications for transportation policies. *Journal of modern transportation* **24**, **4**, 284-303.

Bengler, K., Dietmayer, K., Farber, B., Maurer, M., Stiller, C. and Winner, H. (2014). Three decades of driver assistance systems: Review and future perspectives. *IEEE Intelligent transportation systems magazine* **6**, **4**, 6-22.

Brannstrom, M., Sjoberg, J. and Coelingh, E. (2008). A situation and threat assessment algorithm for a rear-end collision avoidance system. *Proc. IEEE Intelligent Vehicles Symposium*, Eindhoven, Netherlands.

Choi, J., Yi, K., Suh, J. and Ko, B. (2014). Coordinated control of motor-driven power steering torque overlay and differential braking for emergency driving support. *IEEE Tran. Vehicular Technology* **63**, **2**, 566-579.

Choi, M., Oh, J.J. and Choi, S.B. (2013). Linearized recursive least squares methods for real-time identification of tire-road friction coefficient. *IEEE Trans. Vehicular Technology* **62**, **7**, 2906–2918.

Choi, M. and Choi, S.B. (2014). Model predictive control for vehicle yaw stability with practical concerns. *IEEE Trans. Vehicular Technology* **63**, **8**, 3539-3548.

Cui, Q., Ding, R., Wu, X. and Zhou, B. (2019). A new strategy for rear-end collision avoidance via autonomous steering and differential braking in highway driving. *Vehicle system dynamics* **58**, **6**, 955-986.

Diederichs, F., Schüttke, T. and Spath, D. (2015). Driver intention algorithm for pedestrian protection and automated emergency braking systems. *Proc. IEEE 18th International Conference on Intelligent Transportation Systems*, Gran Canaria, Spain.

Funke, J., Brown, M., Erlien, S.M. and Gerdes, J.C. (2016). Collision avoidance and stabilization for autonomous vehicles in emergency scenarios. *IEEE Trans. Control Systems Technology* **25**, **4**, 1204-1216.

He, X., Liu, Y., Lv, C., Ji, X. and Liu, Y. (2019). Emergency steering control of autonomous vehicle for collision avoidance and stabilisation. *Vehicle system dynamics* **57**, **8**, 1163-1187.

Hestermeyer, T., Bongarth, W. and Dornhege, J.H. (2019). Steering features of the new Ford Focus. *In 9th International Munich Chassis Symposium 2018. 1st edn.* Springer Vieweg. Wiesbaden.

Hsu, Y-H.J. (2009). *Estimation and control of lateral tire forces using steering torque*. Ph.D. dissertation. Stanford University. Stanford, CA.

Hu, C., Wang, Z., Qin, Y., Huang, Y., Wang, J. and Wang, R. (2019). Lane keeping control of autonomous vehicles with prescribed performance considering the rollover prevention and input saturation. *IEEE trans. intelligent transportation systems* **21**, **7**, 3091-3103.

Huang, Y. and Chen, Y. (2020). Vehicle lateral stability control based on shiftable stability regions and dynamic margins. *IEEE trans. vehicular technology* **69**, **12**, 14727-14738.

Inagaki, S., Kushiro, I. and Yamamoto, M. (1995). Analysis on vehicle stability in critical cornering using phase-plane method. *Jsae Review* **2**, **16**, 216.

Jansson, J. (2005). *Collision Avoidance Theory: With application to automotive collision mitigation*. Ph.D. dissertation. Linköping University. Linköping, Sweden.

Kim, H., Shin, K., Chang, I. and Huh, K. (2018). Autonomous emergency braking considering road slope and friction coefficient. *Int. J. Automotive Technology* **19**, **6**, 1013-1022.

Lie, A., Tingvall, C., Krafft, M. and Kullgren, A., 2006. The effectiveness of electronic stability control (ESC) in reducing real life crashes and injuries. *Traffic injury prevention* **7**, **1**, 38-43.

Mirzaei, M. and Mirzaeinejad, H. (2012). Optimal design of a non-linear controller for anti-lock braking system. *Transportation research part C: emerging technologies* **24**, 19-35.

Pacejka, H. B. (2006). *Tyre and Vehicle Dynamics*. 2nd edn. Elsevier. Oxford.

Rajamani, R. (2012). *Vehicle Dynamics and Control*. 2nd edn. Springer. London.

Serial#Given by KSAE

Wang, L. (2009). *Model predictive control system design and implementation using MATLAB®*. Springer Science & Business Media. Berlin.

Yi, J., Alvarez, L. and Horowitz, R. (2002). Adaptive emergency braking control with underestimation of friction coefficient. *IEEE Trans. Control Systems Technology* **10**, **3**, 381-392.

Zhai, L., Sun, T. and Wang, J. (2016). Electronic stability control based on motor driving and braking torque distribution for a four in-wheel motor drive electric vehicle. *IEEE Trans. Vehicular Technology* **65**, **6**, 4726-4739.